CHALMERS
UNIVERSITY OF TECHNOLOGY

Location and Map-Assisted Wideband Phase and Time Calibration Between Distributed Antennas

Location and Map-Assisted Wideband Phase and Time Calibration Between Distributed Antennas

Yibo Wu*†, Musa Furkan Keskin†, Ulf Gustavsson*,
Gonzalo Seco-Granados‡, Erik G. Larsson§, and Henk Wymeersch†
*Ericsson Research, Gothenburg, Sweden, †Chalmers University of Technology, Gothenburg, Sweden,
‡Universitat Autonoma de Barcelona, Barcelona, Spain, §Linköping University, Linköping, Sweden

***Abstract*—Distributed massive multiple-input multiple-output networks utilize a large number of distributed access points (APs) to serve multiple user equipments (UEs), offering significant potential for both communication and localization. However, these networks require frequent phase and time calibration between distributed antennas due to oscillator phase drifts, crucial for reciprocity-based coherent beamforming and accurate localization. While this calibration is typically performed through bi-directional measurements between antennas, it can be simplified to uni-directional measurement under perfect knowledge of antenna locations. This paper extends a recent phase calibration narrowband line-of-sight (LoS) model to a phase and time calibration wideband orthogonal frequency division multiplexing model, including both LoS and reflection paths and allowing for joint phase and time calibrations. We explore different scenarios, considering whether or not prior knowledge of antenna locations and the map is available. For each case, we introduce a practical maximum likelihood estimator and conduct Cramér-Rao lower bound (CRLB) analyses to benchmark performance. Simulations validate our estimators against the CRLB in these scenarios.**

***Index Terms*—Time Calibration, phase calibration, cell-free massive MIMO, distributed antenna, reciprocity calibration, carrier phase positioning, delay estimation**

I. Introduction

Distributed massive multiple-input multiple-output (mMIMO) is a promising technology for next-generation communication systems, where numerous distributed access points (APs) serve multiple user equipments (UEs) with uniform service [1], [2]. However, it requires precise phase and time synchronization between APs, critical for uplink combining, downlink MIMO beamforming, and localization [1]–[4]. Bi-directional over-the-air (OtA) measurements between the antennas of different APs can be used to calibrate uplink-downlink reciprocity phase errors for reciprocity-based beamforming [5]. Unless the local oscillators (LOs) in different APs are mutually locked to each other, the phase drift originating from LO noise requires frequent (millisecond-level) re-calibration [6]–[8]. Such calibration can also be accomplished using bi-directional OtA measurements *between the APs* [3], [8].

This work was supported by the Swedish Foundation for Strategic Research (SSF) under grant no. ID19-0021, the Swedish Research Council under VR grants 2022-03007 and 2023-03414, ELLIIT, the KAW Foundation, and the Spanish Ministry of Science under grant PID2023-152820OB-I00. This work was also conducted within the Advanced Digitalization program at the WiTECH Centre DISCOURSE, financed by VINNOVA and partner companies.

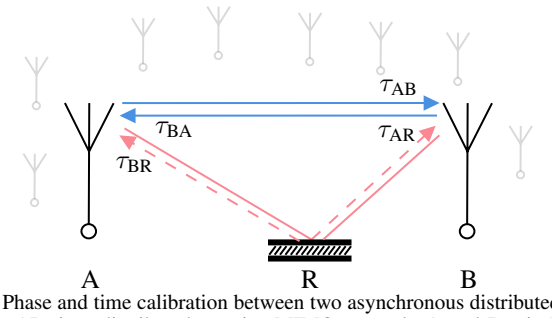

Fig. 1: Phase and time calibration between two asynchronous distributed single-antenna APs in a distributed massive MIMO network, A and B, via LoS and ground reflection paths (reflection point R). Depending on the prior knowledge of the location (AP positions) and map (reflection point position and phase) information, bi-directional or uni-directional measurements are needed.

While [3], [5]–[8] focus on phase calibration issues from hardware impairments and asynchronous timing, time calibration is also crucial for delay-based high-accuracy localization [4], [9], [10]. Joint phase and time calibration, especially addressing errors from imperfect LOs between distributed antennas, remains underexplored. The paper [3] offers a phase calibration method for narrowband transmission over line-of-sight (LoS) channels but does not address time calibration, wideband systems, and multi-path effects (which commonly arise from ground reflections [11]). Additionally, the potential benefits of using location (AP positions) and map information (reflection points and phases) in phase and time calibration are not systematically explored. Specifically, knowing the AP locations reduces the need for calibration from bi-directional to uni-directional measurements, and knowing the map information could enhance calibration accuracy. These research gaps motivate our work.

In this paper, we introduce a novel phase and time calibration signal model for wideband distributed antenna systems, enabling joint phase and time calibration for precise calibration and accurate localization. We investigate various scenarios, considering the availability of location (AP positions) and/or map information (reflection position and phase), over both LoS and reflection paths. We derive maximum likelihood (ML)-based estimators for each scenario to solve the calibration problem. Additionally, we provide a rigorous Cramér-Rao lower bound (CRLB) analysis using Fisher information, establishing a theoretical benchmark for performance evaluation. By examining a setup with two single-antenna APs, we emphasize that our model and techniques apply also to calibration between

antennas of multi-antenna APs and between APs and UEs in distributed mMIMO scenarios, broadening the potential impact of our work.

II. System Model

A. Phase and Clock Offsets

Two single-antenna APs A and B are shown in Fig. 1. Each AP, A or B, has a transmit and receive branch, causing respective time and phase offsets [7]. We assume that each AP has already individually calibrated its transmit and receive antenna times and phases.[1] The rest of this paper focuses on phase and time calibration between different antennas.

The propagation delay between A and B is

$$\tau_{\text{AB}} = \|\boldsymbol{p}_{\text{A}} - \boldsymbol{p}_{\text{B}}\|/c, \tag{1}$$

where $\boldsymbol{p}_{\text{A}}$ and $\boldsymbol{p}_{\text{B}}$ are the 2-D positions of A and B, and c is the speed of light. Note $\tau_{\text{AB}} = \tau_{\text{BA}}$ due to reciprocity. At global time zero, the clock offset for the transmission from A to B is $\delta_{t_{\text{AB}}} \in \mathbb{R}$, and from B to A is $\delta_{t_{\text{BA}}} \in \mathbb{R}$. The additional phase offset transmitting from A to B and from B to A due to hardware impairments (e.g., in-phase and quadrature (IQ) imbalance or common phase error due to phase noise) is denoted by $\delta_{\phi_{\text{AB}}} \in [0, 2\pi)$ and $\delta_{\phi_{\text{BA}}} \in [0, 2\pi)$. We note that

$$\delta_{t_{\text{AB}}} = -\delta_{t_{\text{BA}}}, \tag{2}$$

$$\delta_{\phi_{\text{AB}}} = -\delta_{\phi_{\text{BA}}}. \tag{3}$$

These minus signs arise because a positive transmit time delay shift has the opposite effect on the signal phase compared to a positive receive time delay shift, due to opposite transmission directions. See [7], [8] for more details.

B. Observation Model via LoS Path

We consider an OFDM system with subcarrier spacing Δ_f Hz and N subcarriers. The bandwidth is $W = N\Delta_f$. The additive white Gaussian noise (AWGN) noise power spectral density (PSD) is N_0. The transmit power is P_{tx}. The complex pilot symbol vector at one OFDM symbol, transmitted by AP A, is $\boldsymbol{s}_{\text{A}} = [s_{\text{A}}[0], \cdots, s_{\text{A}}[N-1]]^{\mathsf{T}} \in \mathbb{C}^N$. The average symbol energy $E_s = \mathbb{E}\{|s_{\text{A}}[n]|^2\} = P_{\text{tx}}/W$.

Under an ideal LoS channel, the received symbol at AP B over subcarrier n, after filtering, sampling, and cyclic prefix removal, is given by[2]

$$\begin{aligned} y_{\text{AB}}[n] &= \beta_{\text{AB}} e^{-j\delta_{\phi_{\text{AB}}}} e^{-j2\pi f_c \tilde{\tau}_{\text{AB}}} e^{-j2\pi n \Delta_f \tilde{\tau}_{\text{AB}}} s_{\text{A}}[n] + w_{\text{AB}}[n] \\ &= \beta_{\text{AB}} e^{j\varphi_{\text{AB}}} a(\tilde{\tau}_{\text{AB}})[n] s_{\text{A}}[n] + w_{\text{AB}}[n], \end{aligned} \tag{4}$$

where $\beta_{\text{AB}} \in \mathbb{R}$ is channel gain including path loss, $w_{\text{AB}}[n] \sim \mathcal{N}_{\mathbb{C}}(0, N_0)$ is AWGN. The delay τ_{AB}, pseudo-delay $\tilde{\tau}_{\text{AB}}$ (including the clock offset), carrier phase φ_{AB}, and delay steering vector element $[\boldsymbol{a}(\tilde{\tau}_{\text{AB}})]_n$, are

$$\tilde{\tau}_{\text{AB}} = \tau_{\text{AB}} + \delta_{t_{\text{AB}}}, \tag{5}$$

$$\varphi_{\text{AB}} = -2\pi f_c \tilde{\tau}_{\text{AB}} - \delta_{\phi_{\text{AB}}}, \tag{6}$$

$$[\boldsymbol{a}(\tilde{\tau}_{\text{AB}})]_n = e^{-j2\pi n \Delta_f \tilde{\tau}_{\text{AB}}}. \tag{7}$$

[1]This assumption is valid as the antenna individual calibration can be done using electromagnetic simulations or anechoic chamber measurements [12], or OtA methods [13], [14]. More details on antenna individual calibration definition are in [8].

[2]The model is equivalent to the model in [7, eq. (20)] by setting $\delta_{\phi_{\text{AB}}} = -(\varphi_t - \varphi_r)$ and $\tau_{\text{AB}} = \tau_t - \tau_r$.

where the delay steering vector $\boldsymbol{a}(\tilde{\tau}_{\text{AB}}) \triangleq [[\boldsymbol{a}(\tilde{\tau}_{\text{AB}})]_0, \cdots, [\boldsymbol{a}(\tilde{\tau}_{\text{AB}})]_{N-1}]^{\mathsf{T}} \in \mathbb{C}^N$. Collecting $y_{\text{AB}}[n]$ over N subcarriers gives $\boldsymbol{y}_{\text{AB}} = [y_{\text{AB}}[0], \cdots, y_{\text{AB}}[N-1]]^{\mathsf{T}}$. We obtain (4) in vector form as

$$\boldsymbol{y}_{\text{AB}} = \boldsymbol{\mu}_{\text{AB}} + \boldsymbol{w}_{\text{AB}}, \tag{8}$$

where $\boldsymbol{\mu}_{\text{AB}} \triangleq \beta_{\text{AB}} e^{j\varphi_{\text{AB}}} \boldsymbol{a}(\tilde{\tau}_{\text{AB}}) \odot \boldsymbol{s}_{\text{A}}$, and $\boldsymbol{w}_{\text{AB}} = [w_{\text{AB}}[0], \cdots, w_{\text{AB}}[N-1]]^{\mathsf{T}}$.

Similar to (8), we define the received signals at AP A, transmitted from AP B, as

$$\boldsymbol{y}_{\text{BA}} = \boldsymbol{\mu}_{\text{BA}} + \boldsymbol{w}_{\text{BA}}, \tag{9}$$

where $\boldsymbol{\mu}_{\text{BA}} \triangleq \beta_{\text{BA}} e^{j\varphi_{\text{BA}}} \boldsymbol{a}(\tilde{\tau}_{\text{BA}}) \odot \boldsymbol{s}_{\text{B}}$. The pseudo delay $\tilde{\tau}_{\text{BA}}$ and carrier phase φ_{BA} are

$$\tilde{\tau}_{\text{BA}} = \tau_{\text{BA}} + \delta_{t_{\text{BA}}}, \tag{10}$$

$$\varphi_{\text{BA}} = -2\pi f_c \tilde{\tau}_{\text{BA}} - \delta_{\phi_{\text{BA}}} \tag{11}$$

Note that $\beta_{\text{AB}} = \beta_{\text{BA}}$ and $\tau_{\text{AB}} = \tau_{\text{BA}}$ due to reciprocity.

C. Observation Model via LoS and Reflection Paths

In practice, a pure LoS path from array A to B is not always guaranteed due to multi-path effects like ground reflections. The observation from array A to B, involving a LoS path and a reflection path reflected at a reflection R is represented by

$$\boldsymbol{y}_{\text{AB}} = \boldsymbol{\mu}_{\text{AB}} + \boldsymbol{\mu}_{\text{AR}} + \boldsymbol{w}_{\text{AB}}, \tag{12}$$

where $\boldsymbol{\mu}_{\text{AR}} \triangleq \beta_{\text{AR}} e^{j\varphi_{\text{AR}}} \boldsymbol{a}(\tilde{\tau}_{\text{AR}}) \odot \boldsymbol{s}_{\text{A}}$. The pseudo-delay, $\tilde{\tau}_{\text{AR}}$, and carrier phase, φ_{AR}, of the reflection path are defined as

$$\tilde{\tau}_{\text{AR}} = \tau_{\text{AR}} + \delta_{t_{\text{AB}}}, \tag{13}$$

$$\varphi_{\text{AR}} = -2\pi f_c \tilde{\tau}_{\text{AR}} - \delta_{\phi_{\text{AR}}} - \delta_{\phi_{\text{AB}}}. \tag{14}$$

Here the reflection path delay τ_{AR} is given by $\tau_{\text{AR}} = (||\boldsymbol{p}_{\text{A}} - \boldsymbol{p}_{\text{R}}|| + ||\boldsymbol{p}_{\text{R}} - \boldsymbol{p}_{\text{B}}||)/c$, $\boldsymbol{p}_{\text{R}}$ is the reflection location, and the reflection introduces an unknown phase rotation $\delta_{\phi_{\text{AR}}}$.

Similarly, we can rewrite the observations from AP B to A (8), via a LoS and reflection paths, as

$$\boldsymbol{y}_{\text{BA}} = \boldsymbol{\mu}_{\text{BA}} + \boldsymbol{\mu}_{\text{BR}} + \boldsymbol{w}_{\text{BA}}, \tag{15}$$

where $\boldsymbol{\mu}_{\text{BR}} = \beta_{\text{BR}} e^{j\varphi_{\text{BR}}} \boldsymbol{a}(\tilde{\tau}_{\text{BR}}) \odot \boldsymbol{s}_{\text{B}}$, and the pseudo-delay and carrier phase of the reflection path transmitted from AP B are defined as

$$\tilde{\tau}_{\text{BR}} = \tau_{\text{BR}} + \delta_{t_{\text{BA}}} \tag{16}$$

$$\varphi_{\text{BR}} = -2\pi f_c \tilde{\tau}_{\text{BR}} - \delta_{\phi_{\text{BR}}} - \delta_{\phi_{\text{BA}}}. \tag{17}$$

Note that $\beta_{\text{BR}} = \beta_{\text{AR}}$, the phase rotation $\delta_{\phi_{\text{BR}}} = \delta_{\phi_{\text{AR}}}$, and $\tau_{\text{BR}} = \tau_{\text{AR}}$ due to reciprocity [15].

D. Problem Formulation

The task is to jointly calibrate phase and time between two single-antenna APs using uni-directional (known AP positions) or bi-directional (unknown AP positions) OtA observations. Two scenarios are considered based on the knowledge of AP positions.

- **Known AP positions**: With known positions of APs A and B, we can determine the delay τ_{AB}, which helps to calibrate the phase and clock offsets using uni-directional observation over LoS and reflection paths (if the paths are resolvable), e.g., $\boldsymbol{y}_{\text{AB}}$ from (12). With *unknown map*, i.e., unknown τ_{AR} or $\delta_{\phi_{\text{AR}}}$, and a uni-directional *two-path* observation (12), the unknown parameter vector is defined as

$$\boldsymbol{\eta} = [\delta_{t_{\text{AB}}}, \delta_{\phi_{\text{AB}}}, \tau_{\text{AR}}, \delta_{\phi_{\text{AR}}}, \beta_{\text{AB}}, \beta_{\text{AR}}]^{\mathsf{T}} \in \mathbb{R}^{6\times 1}\ . \tag{18}$$

If the reflection position $\boldsymbol{p}_{\mathrm{R}}$ or the reflection rotation phase $\delta_{\phi_{\mathrm{AR}}}$ is known, i.e., *known map*, the unknown vector $\boldsymbol{\eta}$ in (18) is reduced by excluding τ_{AR} or $\delta_{\phi_{\mathrm{AR}}}$, respectively.
With only a *LoS* path observation, the unknown parameter vector in (18) is reduced to

$$\boldsymbol{\eta} = [\delta_{t_{\mathrm{AB}}}, \delta_{\phi_{\mathrm{AB}}}, \beta_{\mathrm{AB}}]^{\mathsf{T}} \in \mathbb{R}^{3\times 1}. \tag{19}$$

- **Unknown AP positions**: Without knowing the positions of APs A and B, a uni-directional observation, e.g., $\boldsymbol{y}_{\mathrm{AB}}$ from (12), is insufficient to independently estimate both τ_{AB} and $\delta_{t_{\mathrm{AB}}}$, because there are more unknowns (6 in (18) and τ_{AB}) than measurable parameters ($\varphi_{\mathrm{AB}}, \varphi_{\mathrm{AR}}, \tilde{\tau}_{\mathrm{AB}}, \tilde{\tau}_{\mathrm{AR}}, \beta_{\mathrm{AB}}, \beta_{\mathrm{AR}}$). Instead, bi-directional observations $\boldsymbol{y}_{\mathrm{AB}}$ and $\boldsymbol{y}_{\mathrm{BA}}$ are needed. With *unknown map* and bi-directional *two-path* observations, the unknown parameter vector is defined as

$$\boldsymbol{\eta} = [\tau_{\mathrm{AB}}, \delta_{t_{\mathrm{AB}}}, \delta_{\phi_{\mathrm{AB}}}, \tau_{\mathrm{AR}}, \delta_{\phi_{\mathrm{AR}}}, \beta_{\mathrm{AB}}, \beta_{\mathrm{AR}}]^{\mathsf{T}} \in \mathbb{R}^{7\times 1}\ . \tag{20}$$

If the reflection information τ_{AR} and $\delta_{\phi_{\mathrm{AR}}}$ are known, i.e., *known map*, the unknown vector $\boldsymbol{\eta}$ in (20) is reduced by excluding τ_{AR} or $\delta_{\phi_{\mathrm{AR}}}$, respectively.
With only *LoS* path observations, i.e., using observations $\boldsymbol{y}_{\mathrm{AB}}$ from (8) and $\boldsymbol{y}_{\mathrm{BA}}$ (9), the unknown parameter vector is

$$\boldsymbol{\eta} = [\tau_{\mathrm{AB}}, \delta_{t_{\mathrm{AB}}}, \delta_{\phi_{\mathrm{AB}}}, \beta_{\mathrm{AB}}]^{\mathsf{T}} \in \mathbb{R}^{4\times 1}. \tag{21}$$

III. Phase and Time Calibration

This section introduces four novel ML-based estimators for the phase and time calibration tasks (18), (19), (20), and (21) in Section II-D. These estimators share a similar form but differ in their final grid search dimensions.

Proposition 1. *The ML-based estimator of the unknown parameters $\boldsymbol{\eta}$ in* (18)*,* (19)*,* (20)*, and* (21) *are respectively given by*

$$[\hat{\delta}_{t_{AB}}, \hat{\tau}_{AR}, \hat{\delta}_{\phi_{AR}}] = \arg \min_{\substack{\delta_{t_{AB}}, \tau_{AR}, \\ \delta_{\phi_{AR}}}} \mathcal{L}^{Uni}_{2\text{-}path}(\delta_{t_{AB}}, \tau_{AR}, \delta_{\phi_{AR}}), \tag{22}$$

$$\hat{\delta}_{t_{AB}} = \arg \min_{\delta_{t_{AB}}} \mathcal{L}^{Uni}_{LoS}(\delta_{t_{AB}}), \tag{23}$$

$$[\hat{\tau}_{AB}, \hat{\delta}_{t_{AB}}, \hat{\tau}_{AR}, \hat{\delta}_{\phi_{AR}}] = \arg \min_{\substack{\tau_{AB}, \delta_{t_{AB}}, \\ \tau_{AR}, \delta_{\phi_{AR}}}} \mathcal{L}^{Bi}_{2\text{-}path}(\tau_{AB}, \delta_{t_{AB}}, \tau_{AR}, \delta_{\phi_{AR}}), \tag{24}$$

$$[\hat{\tau}_{AB}, \hat{\delta}_{t_{AB}}] = \arg \min_{\tau_{AB}, \delta_{t_{AB}}} \mathcal{L}^{Bi}_{LoS}(\tau_{AB}, \delta_{t_{AB}}), \tag{25}$$

where (22) *and* (23) *are the two-path and LoS estimators using the uni-directional observation $\boldsymbol{y}_{AB}$ from* (12) *and* (8)*, respectively.* (24) *and* (25) *are the two-path and LoS estimators using the bi-directional observations $\boldsymbol{y} = [\boldsymbol{y}^{\mathsf{T}}_{AB}, \boldsymbol{y}^{\mathsf{H}}_{BA}]^{\mathsf{T}}$, obtained from* (12) *and* (15)*, and from* (8) *and* (9)*, respectively. The negative log-likelihood functions (NLLFs) $\mathcal{L}^{Uni}_{2\text{-}path}$, $\mathcal{L}^{uni}_{LoS}$, $\mathcal{L}^{Bi}_{2\text{-}path}$, and $\mathcal{L}^{Bi}_{2\text{-}path}$ share a similar form as*

$$\mathcal{L}_{ML}(\cdot) = \|\ddot{\boldsymbol{y}}\|_2^2 + \|\ddot{\boldsymbol{c}}\|_2^2 - 2\left|\ddot{\boldsymbol{c}}^{\mathsf{H}}\ddot{\boldsymbol{y}}\right|, \tag{26}$$

where, based on the specific estimator, $\mathcal{L}_{ML} = \{\mathcal{L}^{Uni}_{2\text{-}path}, \mathcal{L}^{Uni}_{LoS}, \mathcal{L}^{Bi}_{2\text{-}path}, \mathcal{L}^{Bi}_{LoS}\}$, $\ddot{\boldsymbol{y}}$ and $\ddot{\boldsymbol{c}}$ in (26) *are substituted accordingly to obtain the respective NLLF functions in* (46)*,* (47)*,* (42)*, and* (48)*.*

Proof. The detailed derivation of (24) is given in Appendix A. The derivation of other three estimators follows similar steps, given in Appendix B. □

Analytically solving (22), (23), (24), and (25) is infeasible. Thus, a practical approach is to perform a grid search over the 3-D, 1-D, 4-D, and 2-D parameter spaces for (22), (23), (24), and (25), respectively.

IV. Cramér-Rao Lower Bound and Analysis

Next, we derive the CRLB for parameters in (18), (19), (20), and (21), respectively. The CRLB on the error variance of any unbiased estimator of the unknown parameters $\boldsymbol{\eta}$ is defined as

$$\mathbb{E}_{\boldsymbol{\eta}}\{(\hat{\boldsymbol{\eta}} - \boldsymbol{\eta})(\hat{\boldsymbol{\eta}} - \boldsymbol{\eta})^{\mathsf{T}}\} \geq (\boldsymbol{J}_{\boldsymbol{\eta}})^{-1}. \tag{27}$$

The Fisher information matrix (FIM) of $\boldsymbol{\eta}$ can be calculated as

$$[\boldsymbol{J}_{\boldsymbol{\eta}}]_{i,j} = 2\Re\Big\{\frac{\partial \boldsymbol{\mu}^{\mathsf{H}}}{\partial [\boldsymbol{\eta}]_i}\frac{\partial \boldsymbol{\mu}}{\partial [\boldsymbol{\eta}]_j}\Big\}\frac{1}{N_0}, \tag{28}$$

where $\boldsymbol{\mu}$ is chosen as $[\boldsymbol{\mu}^{\mathsf{T}}_{\mathrm{AB}} + \boldsymbol{\mu}^{\mathsf{T}}_{\mathrm{AR}}]^{\mathsf{T}}$, $\boldsymbol{\mu}_{\mathrm{AB}}$, and $[\boldsymbol{\mu}^{\mathsf{T}}_{\mathrm{AB}}, \boldsymbol{\mu}^{\mathsf{H}}_{\mathrm{BA}}]^{\mathsf{T}}$ for the unknown parameters $\boldsymbol{\eta}$ from (18), (19), and (21), respectively. Using the FIM for an unknown parameter vector $\boldsymbol{\eta}$, we calculate the lower bound on the error variance for the i-th parameter as

$$\mathrm{var}(\hat{\eta}_i) \geq [\boldsymbol{J}^{-1}_{\boldsymbol{\eta}}]_{i,i}. \tag{29}$$

A. Known Positions with LoS Path or Two-path

1) LoS Path

In the scenario with known AP positions and uni-directional observation (8) over LoS path, the analytical CRLBs of the error variance of the unknown $\hat{\delta}_{t_{\mathrm{AB}}}$ and $\hat{\delta}_{\phi_{\mathrm{AB}}}$ from (19) are

$$\mathrm{var}(\hat{\delta}_{t_{\mathrm{AB}}}) = [\boldsymbol{J}^{-1}_{\boldsymbol{\eta}}]_{1,1} = 3/(2\pi^2 W^2 \mathrm{SNR}), \tag{30}$$

$$\mathrm{var}(\hat{\delta}_{\phi_{\mathrm{AB}}}) = [\boldsymbol{J}^{-1}_{\boldsymbol{\eta}}]_{2,2} = 6f_c^2/(W^2\mathrm{SNR}) + 1/(2\mathrm{SNR}), \tag{31}$$

where the $\mathrm{SNR} \triangleq E_s\beta^2 N/N_0$. We omit the derivation details for simplicity. The CRLB for $\hat{\delta}_{t_{\mathrm{AB}}}$ (30) shows that increasing the bandwidth can reduce the estimation error to zero. In contrast, the CRLB for $\hat{\delta}_{\phi_{\mathrm{AB}}}$ (31) indicates a performance threshold. Referring to Eq. (6), this occurs because, with perfectly known $\delta_{t_{\mathrm{AB}}}$, the error in the estimation of $\delta_{\phi_{\mathrm{AB}}}$ is independent of bandwidth and only depends on SNR.

2) Two-path

In the scenario with known AP positions and uni-directional observation (12) over two paths (LoS and reflection), the CRLBs of the error variance of unknown parameters in $\boldsymbol{\eta}$ from (18) is given in Appendix C.

B. Unknown Positions with LoS Path or Two-path

1) LoS Path

The analytical CRLBs of the error variance of $\hat{\tau}_{\mathrm{AB}}$, $\hat{\delta}_{t_{\mathrm{AB}}}$, and $\hat{\delta}_{\phi_{\mathrm{AB}}}$, from (21), are

$$\mathrm{var}(\hat{\tau}_{\mathrm{AB}}) \geq [\boldsymbol{J}^{-1}_{\boldsymbol{\eta}}]_{1,1} = 1/\big((16\pi^2 f_c^2 + 4\pi^2/3)\mathrm{SNR}\big) \tag{32}$$

$$\mathrm{var}(\hat{\delta}_{t_{\mathrm{AB}}}) \geq [\boldsymbol{J}^{-1}_{\boldsymbol{\eta}}]_{2,2} = 3/(4\pi^2 W^2 \mathrm{SNR}), \tag{33}$$

$$\mathrm{var}(\hat{\delta}_{\phi_{\mathrm{AB}}}) \geq [\boldsymbol{J}^{-1}_{\boldsymbol{\eta}}]_{2,2} = 3f_c^2/(W^2\mathrm{SNR}) + 1/(4\mathrm{SNR}). \tag{34}$$

We omit the derivation details for simplicity. Comparing (33) and (34) with the uni-directional CRLBs, (30) and (31), bi-directional observations halve the estimation variances of $\delta_{t_{\mathrm{AB}}}$ and $\delta_{\phi_{\mathrm{AB}}}$. Specifically, (32) shows that the estimation variance

TABLE I: Simulation parameters.

Parameter	Value
$\boldsymbol{p}_{\mathrm{A}}, \boldsymbol{p}_{\mathrm{B}}, \boldsymbol{p}_{\mathrm{R}}$	$[50, 50], [0, 0], [0, -10]$ m
P_{tx}, N_0, f_c, Δ_f	10 mW, -174 dBm/Hz, 2 GHz, 60 kHz
$\delta_{t_{\mathrm{AB}}}$, $\delta_{\phi_{\mathrm{AB}}}$, $\delta_{\phi_{\mathrm{AR}}}$	0.67μs, 10°, 20°
β_{AB}, β_{AR}	$\lambda/(4\pi \|\boldsymbol{p}_{\mathrm{A}} - \boldsymbol{p}_{\mathrm{B}}\|)$, $\lambda/(4\pi \|\|\boldsymbol{p}_{\mathrm{A}} - \boldsymbol{p}_{\mathrm{R}}\| + \|\boldsymbol{p}_{\mathrm{R}} - \boldsymbol{p}_{\mathrm{B}}\|\|)$

TABLE II: Setups of two scenarios and the corresponding estimators.

Setups	Scenario 1	Scenario 2
Prior Localization	Known $\boldsymbol{p}_{\mathrm{A}}$, $\boldsymbol{p}_{\mathrm{B}}$	Unknown $\boldsymbol{p}_{\mathrm{A}}$, $\boldsymbol{p}_{\mathrm{B}}$
Unknown parameters $\boldsymbol{\eta}$	Two-path: (18), LoS: (19)	Two-path:(20), LoS:(21)
Prior Map in two-path	Reduced $\boldsymbol{\eta}$ (18)	Reduced $\boldsymbol{\eta}$ (20)
Estimators	Two-path est.:(22), LoS est.:(23)	LoS est.:(25)

of τ_{AB} decreases with f_c^2, unlike $\delta_{t_{\mathrm{AB}}}$ and $\delta_{\phi_{\mathrm{AB}}}$. This is because $\delta_{t_{\mathrm{AB}}}$ and $\delta_{\phi_{\mathrm{AB}}}$ can somehow be canceled out due to their opposite signs in the carrier phases of bi-directional measurements: i.e., $-\delta_{\phi_{\mathrm{AB}}}$ in φ_{AB} and $+\delta_{\phi_{\mathrm{AB}}}$ in φ_{BA}. The same applies to $\delta_{t_{\mathrm{AB}}}$. This in turn improves the estimation of τ_{AB} due to its same signs in φ_{AB} and φ_{BA}.

2) Two-path

In the scenario with unknown AP positions and bi-directional observation ((12) and (15)) over two paths (LoS and reflection), the CRLBs of the error variance of unknown parameters in $\boldsymbol{\eta}$ from (20) is given in Appendix D.

V. Simulation Results

A. Scenarios

We consider a simulation setup involving two single-antenna APs. The setup parameters, following similar parameters in [4], are given in Table I. The evaluated scenarios and estimators are given in Table II. The ML estimator (24) is not evaluated due to its impractical and costly 4-D grid search.

B. Scenario 1: Calibration with Known AP Positions

1) Impact of Bandwidth

The root-mean-squared errors (RMSEs) on the estimation of clock offset $\hat{\delta}_{t_{\mathrm{AB}}}$ and phase offset $\hat{\delta}_{\phi_{\mathrm{AB}}}$ versus bandwidth W are shown in Fig. 2 and Fig. 3, averaged over 50 Monte Carlo simulations. The corresponding CRLBs are given in solid lines. The results indicate that the proposed ML-based estimators can nearly reach the corresponding CRLBs. Fine-tuning the grid search size can further improve their stability. With unknown map, the reflection path degrades the two-path estimator's performance compared to only LoS estimator on LoS path model. This degradation lessens with growing bandwidths, which allows a better resolution between LoS and reflection paths (delay difference in Hz: $1/(\tau_{\mathrm{AR}} - \tau_{\mathrm{AB}}) \approx 17$ MHz). With known map, the two-path estimator performs better than the LoS estimator for larger bandwidths (> 30 MHz), showing a nonlinear improvement with bandwidth. The LoS estimator performs poorly under the two-path model due to mismatched estimators. The two-path estimators' phase offset RMSEs deviates from the CRLB for small bandwidths (< 20 MHz) because of phase wrapping. The RMSE values in Fig. 3 are larger than those in Fig. 2, aligning with (30) and (31).

2) NLLF Results

Fixing the bandwidth $W = 12$ MHz, Fig. 4 shows the clock offset estimation error, $(\hat{\delta}_{t_{\mathrm{AB}}} - \delta_{t_{\mathrm{AB}}}) \times c$ measured in distance,

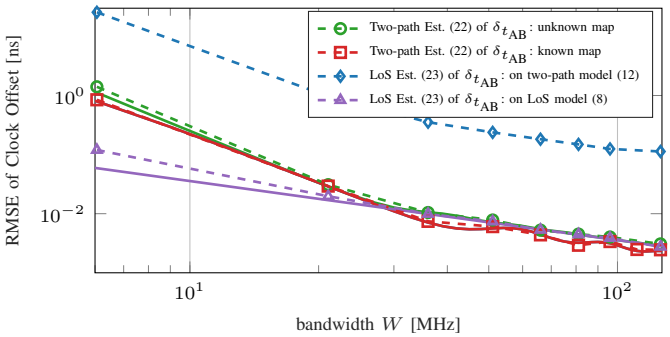

Fig. 2: RMSE of the clock offset estimate $\delta_{t_{\mathrm{AB}}}$ in ns versus the bandwidth for various estimators for the scenario with known AP positions. Solid lines are the corresponding CRLBs.

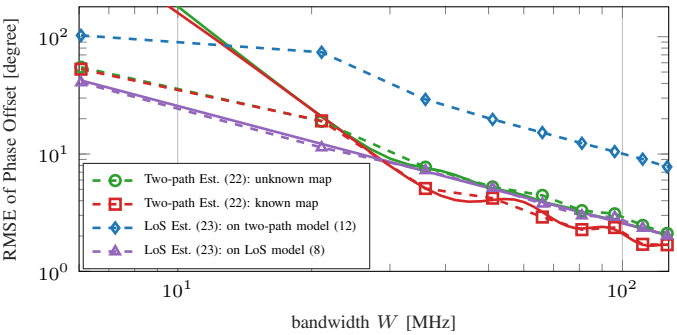

Fig. 3: RMSE of the phase offset estimate $\delta_{\phi_{\mathrm{AB}}}$ in degree versus the bandwidth for various estimators for the scenario with known AP positions.

which is a 1D slice of the 3D NLLF results, fixing the other two parameters, for the two-path estimator (22) and the 1D NLLF of the LoS estimator (23). The LoS estimator (23) shows inferior performance under the two-path observation model (12) due to interference from the reflection path. In contrast, the two-path estimator (22) with unknown reflection parameters offers better accuracy. Having knowledge of reflection path parameters offers almost no advantage because of the limited bandwidth of 12 MHz. The LoS estimator is most effective under the LoS observation model (8), displaying the sharpest NLLF curve near the ground truth. The results demonstrate the superior performance of the proposed estimators, highlighting the importance of a precise multi-path model over map data for calibration accuracy.

C. Scenario 2: Calibration with Unknown AP Positions

Fig. 5 shows the RMSEs on the estimation of clock offset $\delta_{\tau_{\mathrm{AB}}}$ and delay τ_{AB} versus bandwidth W for the LoS estimator (25) under unknown AP positions and bi-directional observations over LoS and two-path channel. The results of the LoS estimator (23) using uni-directional observation from Fig. 2 is also shown. The corresponding CRLBs are given in solid lines.

As bandwidth increases, the performance of both LoS estimators for clock offset $\delta_{\tau_{\mathrm{AB}}}$ improves linearly. The bi-directional LoS estimator (25) halves the estimation error, as discussed by the CRLB analysis in Section IV-B. The delay estimation τ_{AB} demonstrates a threshold effect where, with sufficiently large bandwidth (> 100 MHz), the estimation can approach its CRLB at a much lower level (see right y-axis) due to carrier phase exploitation, similar to the threshold effect discussed in [10]. The two-path measurements have a negligible effect on

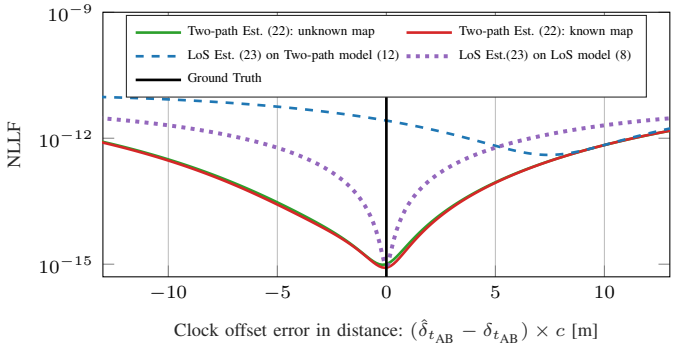

Fig. 4: 1-D snapshot of NLLF results for clock offset error in distance using 3-D and 1-D search for two-path and LoS estimators, given known AP positions. Signal bandwidth $W = 12$ MHz.

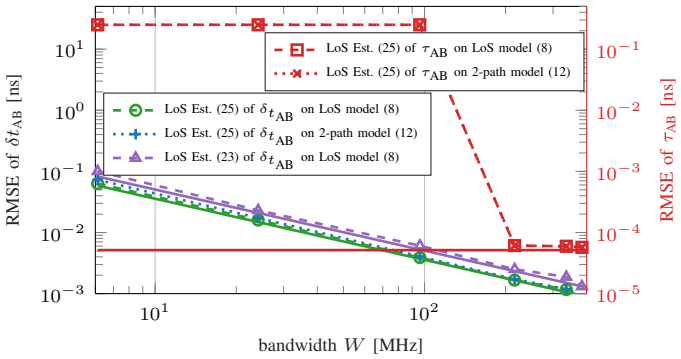

Fig. 5: RMSE on the estimation of the clock offset $\hat{\delta}_{t_{\text{AB}}}$ (left y-axis) and delay $\hat{\tau}_{\text{AB}}$ (right y-axis) versus the bandwidth for two LoS estimators, (23) and (46), in scenarios with and without known AP positions and LoS path.

the bi-directional LoS estimator (25) for both clock offset and delay, in contrast to the significant impact on the uni-directional LoS estimator (23), as illustrated in Fig. 2 and Fig. 4, mainly because bi-directional measurements help to decouple reflection parameters from LoS parameters. For instance, $\delta_{\phi_{\text{AB}}}$ changes signs in (12) and (15), unlike τ_{AR} and $\delta_{t_{\text{AB}}}$.

This threshold effect arises due to the integer ambiguity error (41) in the phase offset estimation when exploiting the carrier phase. Fig. 6 shows the 1-D extraction from the 2-D NLLF results of the estimator (25) for delay estimation at 50 MHz and 200 MHz. With larger bandwidths, a distinct global optimum correctly identifies the optimum, while smaller bandwidths lead to numerous local optima and incorrect estimates. Mismatched two-path measurements on the LoS estimator show that the large bandwidth advantage is less apparent compared to the cases without mismatch.

VI. Conclusion

This paper addresses phase and time calibration in distributed mMIMO context using a wideband multi-path model for separate phase and time offsets calibration. We cover scenarios with/without known AP positions and/or reflection information, offering a practical framework. We developed ML estimators for each scenario. Our CRLB analyses establish theoretical performance benchmarks, improving the understanding of calibration limits. Extensive simulations validated our estimators against the CRLBs. Focusing on two single-antenna APs, we note that our model and techniques are applicable to intra-AP and AP-

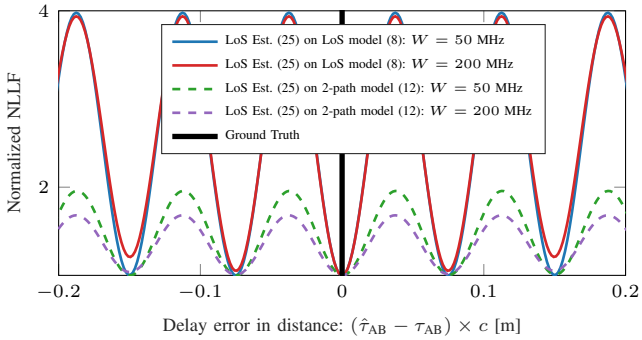

Fig. 6: 1-D snapshot of 2-D NLLF results for delay estimate error in distance for the LoS estimators and (25).

UE calibration in distributed massive MIMO. Future work can explore calibration with unknown AP positions in a multi-path channel and localization with multiple APs.

Appendix A
Proof of (24) in Proposition 1

Using the ML criterion, we solve the estimation of $\boldsymbol{\eta}$ from (21) using the bi-directional two-path observation $\boldsymbol{y} = [\boldsymbol{y}_{\text{AB}}^{\mathsf{T}}, \boldsymbol{y}_{\text{BA}}^{\mathsf{H}}]^{\mathsf{T}} \in \mathbb{C}^{2N}$ from (12) and (15) as

$$\hat{\boldsymbol{\eta}} = \arg\max_{\boldsymbol{\eta}} \quad p(\boldsymbol{y}|\boldsymbol{\eta}). \tag{35}$$

Denote $\boldsymbol{\mu}_{\text{AB-BA}} \triangleq [\boldsymbol{\mu}_{\text{AB}}^{\mathsf{T}}, \boldsymbol{\mu}_{\text{BA}}^{\mathsf{H}}]^{\mathsf{T}} \in \mathbb{C}^{2N}$, and $\boldsymbol{\mu}_{\text{R}} \triangleq [\boldsymbol{\mu}_{\text{AR}}^{\mathsf{T}}, \boldsymbol{\mu}_{\text{BR}}^{\mathsf{H}}]^{\mathsf{T}} \in \mathbb{C}^{2N}$. Solving (35) is equivalent to minimize the negative log-likelihood version of $p(\boldsymbol{y}|\boldsymbol{\eta})$. After removing irrelevant terms in $\log p(\boldsymbol{y}|\boldsymbol{\eta})$, the problem in (35) becomes to minimize the NLLF, given by $\hat{\boldsymbol{\eta}} = \arg\min_{\boldsymbol{\eta}} \quad \mathcal{L}_{\text{ML}}(\boldsymbol{\eta})$, where

$$\begin{aligned}
\mathcal{L}_{\text{ML}}(\boldsymbol{\eta}) &\triangleq \|\boldsymbol{y} - \boldsymbol{\mu}_{\text{AB-BA}} - \boldsymbol{\mu}_{\text{R}}\|_2^2 \\
&= \Big\| \boldsymbol{y} - \beta_{\text{AB}}[e^{-j\delta_{\phi_{\text{AB}}}} e^{j\tilde{\varphi}_{\text{AB}}} \boldsymbol{c}_{\text{AB}}^{\mathsf{T}}, e^{j\delta_{\phi_{\text{BA}}}} e^{-j\tilde{\varphi}_{\text{BA}}} \boldsymbol{c}_{\text{BA}}^{\mathsf{H}}]^{\mathsf{T}} \\
&\qquad - \beta_{\text{AR}}[e^{-j\delta_{\phi_{\text{AB}}}} e^{j\tilde{\varphi}_{\text{AR}}} \boldsymbol{c}_{\text{AR}}^{\mathsf{T}}, e^{j\delta_{\phi_{\text{BA}}}} e^{-j\tilde{\varphi}_{\text{BR}}} \boldsymbol{c}_{\text{BR}}^{\mathsf{H}}]^{\mathsf{T}} \Big\|_2^2, \qquad (36) \\
&= \Big\| \boldsymbol{y} - \beta_{\text{AB}} e^{-j\delta_{\phi_{\text{AB}}}} \boldsymbol{c}_{\text{AB-BA}} - \beta_{\text{AR}} e^{-j\delta_{\phi_{\text{AB}}}} \boldsymbol{c}_{\text{AR-BR}} \Big\|_2^2, \qquad (37)
\end{aligned}$$

where $\tilde{\varphi}_{\text{AB}} \triangleq \varphi_{\text{AB}} - \delta_{\phi_{\text{AB}}}$, $\tilde{\varphi}_{\text{BA}} \triangleq \varphi_{\text{BA}} - \delta_{\phi_{\text{BA}}}$, $\tilde{\varphi}_{\text{AR}} \triangleq \varphi_{\text{AR}} - \delta_{\phi_{\text{AB}}}$, $\tilde{\varphi}_{\text{BR}} \triangleq \varphi_{\text{BR}} - \delta_{\phi_{\text{BR}}}$, $\boldsymbol{c}_{\text{AB-BA}} \triangleq [e^{j\tilde{\varphi}_{\text{AB}}} \boldsymbol{c}_{\text{AB}}^{\mathsf{T}}, e^{-j\tilde{\varphi}_{\text{BA}}} \boldsymbol{c}_{\text{BA}}^{\mathsf{H}}]^{\mathsf{T}}$, $\boldsymbol{c}_{\text{AR-BR}} \triangleq [e^{j\tilde{\varphi}_{\text{AR}}} \boldsymbol{c}_{\text{AR}}^{\mathsf{T}}, e^{-j\tilde{\varphi}_{\text{BR}}} \boldsymbol{c}_{\text{BR}}^{\mathsf{H}}]^{\mathsf{T}}$, and from (36) to (37) we use $\delta_{\phi_{\text{AB}}} = -\delta_{\phi_{\text{BA}}}$ (defined in (3)).

We can express two channel gains in vector form as $\boldsymbol{\beta} = [\beta_{\text{AB}}, \beta_{\text{AR}}]^{\mathsf{T}}$. Thus we can rewrite (37) as

$$\mathcal{L}_{\text{ML}}(\boldsymbol{\eta}) = \Big\| \boldsymbol{y} - e^{-j\delta_{\phi_{\text{AB}}}} \boldsymbol{C}_{\text{A-R-B}} \boldsymbol{\beta}, \Big\|_2^2, \tag{38}$$

where $\boldsymbol{C}_{\text{A-R-B}} \triangleq [\boldsymbol{c}_{\text{AB-BA}}, \boldsymbol{c}_{\text{AR-BR}}] \in \mathbb{C}^{2N \times 2}$. To solve this ML estimation problem, we first estimate $\boldsymbol{\beta}$ as a function of the remaining parameters in closed-form as

$$\begin{aligned}
\hat{\boldsymbol{\beta}}^{\text{ML}} &= \Re\big\{ \big(\boldsymbol{C}_{\text{A-R-B}}^{\mathsf{H}} \boldsymbol{C}_{\text{A-R-B}}\big)^{-1} (e^{-j\delta_{\phi_{\text{AB}}}} \boldsymbol{C}_{\text{A-R-B}})^{\mathsf{H}} \boldsymbol{y} \big\} \\
&= \frac{1}{2} \big(\boldsymbol{C}_{\text{A-R-B}}^{\mathsf{H}} \boldsymbol{C}_{\text{A-R-B}}\big)^{-1} (e^{-j\delta_{\phi_{\text{AB}}}} \boldsymbol{C}_{\text{A-R-B}})^{\mathsf{H}} \boldsymbol{y} \\
&\quad + \frac{1}{2} \Big(\boldsymbol{y}^{\mathsf{H}} (e^{-j\delta_{\phi_{\text{AB}}}} \boldsymbol{C}_{\text{A-R-B}}) \big(\boldsymbol{C}_{\text{A-R-B}}^{\mathsf{H}} \boldsymbol{C}_{\text{A-R-B}}\big)^{-1} \Big)^{\mathsf{T}}. \qquad (39)
\end{aligned}$$

Substituting (39) into (38) drops the dependency of $\boldsymbol{\beta}$, we obtain the compressed loss function

$$\mathcal{L}_{\text{ML}}(\tau_{\text{AB}}, \delta_{\phi_{\text{AB}}}, \delta_{t_{\text{AB}}}, \tau_{\text{AR}}, \delta_{\phi_{\text{AR}}}) = \|\breve{\boldsymbol{y}} - e^{-2j\delta_{\phi_{\text{AB}}}} \breve{\boldsymbol{c}}_{\text{A-R-B}}\|_2^2, \tag{40}$$

where $\breve{\boldsymbol{y}} \triangleq \boldsymbol{y} - \frac{1}{2}\boldsymbol{C}_{\text{A-R-B}}\big(\boldsymbol{C}_{\text{A-R-B}}^{\mathsf{H}}\boldsymbol{C}_{\text{A-R-B}}\big)^{-1}\boldsymbol{C}_{\text{A-R-B}}^{\mathsf{H}}\boldsymbol{y}$ and $\breve{\boldsymbol{c}}_{\text{A-R-B}} \triangleq \frac{1}{2}\boldsymbol{C}_{\text{A-R-B}}\big(\boldsymbol{C}_{\text{A-R-B}}^{\mathsf{H}}\boldsymbol{C}_{\text{A-R-B}}\big)^{-1}\boldsymbol{C}_{\text{A-R-B}}^{\mathsf{T}}(\boldsymbol{y}^{\mathsf{H}})^{T}$. Similarly, we can also estimate $\delta_{\phi_{\text{AB}}}$ in closed-form using the remaining parameters as

$$\hat{\delta}_{\phi_{\text{AB}}} = -\frac{\angle\big(\breve{\boldsymbol{c}}_{\text{A-R-B}}^{\mathsf{H}}\breve{\boldsymbol{y}}\big)}{2} + z_1\pi, \tag{41}$$

where $z_1 \in \mathbb{Z}$ is introduced to account for possible integer ambiguities in phase estimation. Inserting (41) into (40) yields

$$\mathcal{L}_{\text{2-path}}^{\text{Bi}}(\tau_{\text{AB}}, \delta_{t_{\text{AB}}}, \tau_{\text{AR}}, \delta_{\phi_{\text{AR}}}) = \|\breve{\boldsymbol{y}}\|_2^2 + \|\breve{\boldsymbol{c}}_{\text{ABA}}\|_2^2 - 2\left|\breve{\boldsymbol{c}}_{\text{ABA}}^{\mathsf{H}}\breve{\boldsymbol{y}}\right|. \tag{42}$$

Appendix B
Proof of (22), (23), and (25) in Proposition 1

Using the ML criterion, we solve the estimation of $\boldsymbol{\eta}$ from (18), (19), and (21) by minimizing the following NLLFs $\mathcal{L}_{\text{ML}}(\boldsymbol{\eta}) \triangleq$

$$\begin{cases} \|\boldsymbol{y}_{\text{AB}} - \boldsymbol{\mu}_{\text{AB}} - \boldsymbol{\mu}_{\text{AR}}\|_2^2, & \text{for } \boldsymbol{\eta} \text{ in (18), } \boldsymbol{y}_{\text{AB}} \text{ in (12)} \quad (43) \\ \|\boldsymbol{y}_{\text{AB}} - \boldsymbol{\mu}_{\text{AB}}\|_2^2, & \text{for } \boldsymbol{\eta} \text{ in (19), } \boldsymbol{y}_{\text{AB}} \text{ in (8)} \quad (44) \\ \|\boldsymbol{y} - \boldsymbol{\mu}_{\text{AB-BA}}\|_2^2, & \text{for } \boldsymbol{\eta} \text{ in (21), } \boldsymbol{y} \text{ in (8), (9),} \quad (45) \end{cases}$$

where the bi-directional LoS observation $\boldsymbol{y} = [\boldsymbol{y}_{\text{AB}}^{\mathsf{T}}, \boldsymbol{y}_{\text{BA}}^{\mathsf{H}}]^{\mathsf{T}} \in \mathbb{C}^{2N}$ in (45) is obtained from (8) and (9).

We omit some details for simplicity and follow similar steps from (36) to (41) to compress the unknown β_{AB}, β_{BA} (if applicable), β_{AR} (if applicable), β_{BR} (if applicable), and $\delta_{\phi_{\text{AB}}}$ in each NLLF function in (43), (44), and (45). Specifically, we obtain the compressed loss function of (43) for the uni-directional two-path estimator,

$$\mathcal{L}_{\text{2-path}}^{\text{Uni}}(\delta_{t_{\text{AB}}}, \tau_{\text{AR}}, \delta_{\phi_{\text{AR}}}) = \|\breve{\boldsymbol{y}}_{\text{AB}}\|_2^2 + \|\breve{\boldsymbol{c}}_{\text{ABR}}\|_2^2 - 2\left|\breve{\boldsymbol{c}}_{\text{ABR}}^{\mathsf{H}}\breve{\boldsymbol{y}}_{\text{AB}}\right|, \tag{46}$$

where $\breve{\boldsymbol{y}}_{\text{AB}} \triangleq \boldsymbol{y}_{\text{AB}} - \frac{1}{2}\boldsymbol{C}_{\text{ABR}}\big(\boldsymbol{C}_{\text{ABR}}^{\mathsf{H}}\boldsymbol{C}_{\text{ABR}}\big)^{-1}\boldsymbol{C}_{\text{ABR}}^{\mathsf{H}}\boldsymbol{y}_{\text{AB}}$ and $\breve{\boldsymbol{c}}_{\text{ABR}} \triangleq \frac{1}{2}\boldsymbol{C}_{\text{ABR}}\big(\boldsymbol{C}_{\text{ABR}}^{\mathsf{H}}\boldsymbol{C}_{\text{ABR}}\big)^{-1}\boldsymbol{C}_{\text{ABR}}^{\mathsf{T}}(\boldsymbol{y}_{\text{AB}}^{\mathsf{H}})^{T}$, $\boldsymbol{C}_{\text{ABR}} \triangleq [e^{j\tilde{\varphi}_{\text{AB}}}\boldsymbol{c}_{\text{AB}}, e^{j\tilde{\varphi}_{\text{AR}}}\boldsymbol{c}_{\text{AR}}] \in \mathbb{C}^{N\times 2}$, $\boldsymbol{c}_{\text{AB}} \triangleq \boldsymbol{a}(\tilde{\tau}_{\text{AB}}) \odot \boldsymbol{s}_{\text{A}}$ and $\boldsymbol{c}_{\text{AR}} \triangleq \boldsymbol{a}(\tilde{\tau}_{\text{AR}}) \odot \boldsymbol{s}_{\text{A}}$.

Similarly, we can also obtain the compressed loss function of (44) for the uni-directional LoS estimator,

$$\mathcal{L}_{\text{LoS}}^{\text{Uni}}(\delta_{t_{\text{AB}}}) = \|\acute{\boldsymbol{y}}_{\text{AB}}\|_2^2 + \|\acute{\boldsymbol{c}}_{\text{AB}}\|_2^2 - 2\left|\acute{\boldsymbol{c}}_{\text{AB}}^{\mathsf{H}}\acute{\boldsymbol{y}}_{\text{AB}}\right|, \tag{47}$$

where $\acute{\boldsymbol{y}}_{\text{AB}} \triangleq \boldsymbol{y}_{\text{AB}} - \boldsymbol{c}_{\text{AB}}^{\mathsf{H}}\boldsymbol{y}_{\text{AB}}/2\|\boldsymbol{c}_{\text{AB}}\|_2^2\boldsymbol{c}_{\text{AB}}$ and $\acute{\boldsymbol{c}}_{\text{AB}} \triangleq e^{-j4\pi f_c\tilde{\tau}_{\text{AB}}}\boldsymbol{y}_{\text{AB}}^{\mathsf{H}}\boldsymbol{c}_{\text{AB}}\|\boldsymbol{c}_{\text{AB}}\|_2^2\boldsymbol{c}_{\text{AB}}/2$. We obtain the compressed loss function of (45) for the bi-directional LoS estimator,

$$\mathcal{L}_{\text{LoS}}^{\text{Bi}}(\tau_{\text{AB}}, \delta_{t_{\text{AB}}}) = \|\tilde{\boldsymbol{y}}\|_2^2 + \|\tilde{\boldsymbol{c}}_{\text{ABA}}\|_2^2 - 2\left|\tilde{\boldsymbol{c}}_{\text{ABA}}^{\mathsf{H}}\tilde{\boldsymbol{y}}\right|, \tag{48}$$

where $\tilde{\boldsymbol{y}} \triangleq \boldsymbol{y} - \boldsymbol{c}_{\text{ABA}}^{\mathsf{H}}\boldsymbol{y}\boldsymbol{c}_{\text{ABA}}/\|\boldsymbol{c}_{\text{ABA}}\|_2^2$ and $\tilde{\boldsymbol{c}}_{\text{ABA}} \triangleq \boldsymbol{y}^{\mathsf{H}}\boldsymbol{c}_{\text{ABA}}\boldsymbol{c}_{\text{ABA}}/\|\boldsymbol{c}_{\text{ABA}}\|_2^2$.

Appendix C
CRLB Calculation of $\boldsymbol{\eta}$ from (18).

The FIM of $\boldsymbol{\eta}$ from (18) is calculated following (28) using $\partial\boldsymbol{\mu}/\partial\delta_{t_{\text{AB}}} = \boldsymbol{D}_1\boldsymbol{\mu}$, $\partial\boldsymbol{\mu}/\partial\delta_{\phi_{\text{AB}}} = -j\boldsymbol{\mu}$, $\partial\boldsymbol{\mu}/\partial\tau_{\text{AR}} = \boldsymbol{D}_1\boldsymbol{\mu}_{\text{AR}}$ $\partial\boldsymbol{\mu}/\partial\delta_{\phi_{\text{AR}}} = -j\boldsymbol{\mu}_{\text{AR}}$ $\partial\boldsymbol{\mu}/\partial\beta_{\text{AR}} = \boldsymbol{\mu}_{\text{AR}}/\beta_{\text{AR}}$ $\partial\boldsymbol{\mu}/\partial\beta_{\text{AB}} = \boldsymbol{\mu}_{\text{AB}}/\beta_{\text{AB}}$. Here $\boldsymbol{D}_1 = \text{diag}(\boldsymbol{d}_1)$, and $\boldsymbol{d}_1 = -j2\pi(f_c\mathbf{1}_N + \Delta_f([-(N-1)/2, \cdots, (N-1)/2]))$. Using these derivatives, the corresponding FIM elements can be calculated following (28). Notably, the FIM size is reduced based on prior knowledge of τ_{AR} and $\delta_{\phi_{\text{AR}}}$. Finally, the error covariance bounds for $\delta_{t_{\text{AB}}}$, $\delta_{\phi_{\text{AB}}}$, τ_{AR}, and $\delta_{\phi_{\text{AR}}}$ (if applicable) are obtained following (29).

Appendix D
CRLB Calculation of $\boldsymbol{\eta}$ from (20).

The FIM of $\boldsymbol{\eta}$ from (20) is calculated following (28) using $\boldsymbol{\mu} = (\boldsymbol{\mu}_{\text{AB-BA}} + \boldsymbol{\mu}_{\text{R}})$, defined after (35). The derivatives are $\partial\boldsymbol{\mu}/\partial\tau_{\text{AB}} = \boldsymbol{D}_{1,1}\boldsymbol{\mu}_{\text{AB-BA}}$, $\partial\boldsymbol{\mu}/\partial\delta_{t_{\text{AB}}} = \boldsymbol{D}_{1,2}\boldsymbol{\mu}$, $\partial\boldsymbol{\mu}/\partial\delta_{\phi_{\text{AB}}} = -j\boldsymbol{\mu}$, $\partial\boldsymbol{\mu}/\partial\tau_{\text{AR}} = \boldsymbol{D}_{1,1}\boldsymbol{\mu}_{\text{R}}$, $\partial\boldsymbol{\mu}/\partial\delta_{\phi_{\text{AR}}} = -j\boldsymbol{\mu}_{\text{R}}$, $\partial\boldsymbol{\mu}/\partial\beta_{\text{AR}} = \boldsymbol{\mu}_{\text{R}}/\beta_{\text{AR}}$, $\partial\boldsymbol{\mu}/\partial\beta_{\text{AB}} = \boldsymbol{\mu}_{\text{AB-BA}}/\beta_{\text{AB}}$. Here $\boldsymbol{D}_{1,1} = \text{diag}([\boldsymbol{d_1}, -\boldsymbol{d_1}])$, $\boldsymbol{D}_{1,2} = \text{diag}([\boldsymbol{d_1}, -\boldsymbol{d_2}])$, and $\boldsymbol{d}_2 = -j2\pi(f_c\mathbf{1}_N - \Delta_f\text{diag}([-(N-1)/2, \cdots, (N-1)/2]))$. These derivatives can be used following (28). Notably, the FIM size are reduced based on prior knowledge of τ_{AR} and $\delta_{\phi_{\text{AR}}}$. Finally, the error covariance bounds for each parameter in (20) are obtained following (29).

References

[1] Ö. T. Demir, E. Björnson, and L. Sanguinetti, "Foundations of user-centric cell-free massive MIMO," *Foundations and Trends® in Signal Process.*, vol. 14, no. 3-4, 2021.

[2] H. Q. Ngo, A. Ashikhmin, H. Yang, E. G. Larsson, and T. L. Marzetta, "Cell-free massive MIMO versus small cells," *IEEE Trans. Wireless Commun.*, vol. 16, no. 3, pp. 1834–1850, Jan. 2017.

[3] E. G. Larsson, "Massive synchrony in distributed antenna systems," *IEEE Trans. Signal Process.*, vol. 72, pp. 855–866, 2024.

[4] A. Fascista, B. J. Deutschmann, M. F. Keskin, T. Wilding, A. Coluccia, K. Witrisal, E. Leitinger, G. Seco-Granados, and H. Wymeersch, "Uplink joint positioning and synchronization in cell-free deployments with radio stripes," *IEEE ICC Workshop*, 2023 May.

[5] J. Vieira, F. Rusek, O. Edfors, S. Malkowsky, L. Liu, and F. Tufvesson, "Reciprocity calibration for massive MIMO: Proposal, modeling, and validation," *IEEE Trans. Wireless Commun.*, vol. 16, no. 5, pp. 3042–3056, 2017.

[6] Y. Xu, E. G. Larsson, E. A. Jorswieck, X. Li, S. Jin, and T.-H. Chang, "Distributed signal processing for extremely large-scale antenna array systems: State-of-the-art and future directions," *arXiv preprint arXiv:2407.16121*, 2024.

[7] R. Nissel, "Correctly modeling TX and RX chain in (distributed) massive MIMO—New fundamental insights on coherency," *IEEE Commun. Lett.*, vol. 26, no. 10, pp. 2465–2469, 2022.

[8] E. G. Larsson and J. Vieira, "Phase calibration of distributed antenna arrays," *IEEE Commun. Lett.*, 2023.

[9] S. Fan, W. Ni, H. Tian, Z. Huang, and R. Zeng, "Carrier phase-based synchronization and high-accuracy positioning in 5G new radio cellular networks," *IEEE Trans. Commun.*, vol. 70, no. 1, pp. 564–577, 2021.

[10] H. Wymeersch, R. Amiri, and G. Seco-Granados, "Fundamental performance bounds for carrier phase positioning in cellular networks," in *IEEE GLOBECOM*. IEEE, 2023 Dec., pp. 7478–7483.

[11] S. Jaeckel, L. Raschkowski, S. Wu, L. Thiele, and W. Keusgen, "An explicit ground reflection model for mm-wave channels," in *IEEE WCNCW*. IEEE, 2017, pp. 1–5.

[12] L. Sevgi, S. Cakir, and G. Cakir, "Antenna calibration for EMC tests and measurements," *IEEE Antennas Propag. Mag.*, vol. 50, no. 3, pp. 215–224, 2008.

[13] X. Jiang, A. Decurninge, K. Gopala, F. Kaltenberger, M. Guillaud, D. Slock, and L. Deneire, "A framework for over-the-air reciprocity calibration for TDD massive MIMO systems," *IEEE Trans. Wireless Commun.*, vol. 17, no. 9, pp. 5975–5990, 2018.

[14] Y. Cao, P. Wang, K. Zheng, X. Liang, D. Liu, M. Lou, J. Jin, Q. Wang, D. Wang, Y. Huang *et al.*, "Experimental performance evaluation of cell-free massive MIMO systems using COTS RRU with OTA reciprocity calibration and phase synchronization," *IEEE JSAC*, vol. 41, no. 6, pp. 1620–1634, 2023.

[15] Y. Zhang, J. Zhang, X. Chu, and J. Zhang, "Effects of wall reflection on the per-antenna power distribution of ZF-precoded ULA for indoor mmWave MU-MIMO transmissions," *IEEE Communications Letters*, vol. 25, no. 1, pp. 13–17, 2020.